IEEE Access
Multidisciplinary ⋮ Rapid Review ⋮ Open Access Journal

Received August 5, 2021, accepted August 17, 2021, date of publication August 24, 2021, date of current version August 31, 2021.

Digital Object Identifier 10.1109/ACCESS.2021.3107253

UAV Based Satellite-Terrestrial Systems With Hardware Impairment and Imperfect SIC: Performance Analysis of User Pairs

NGOC-LONG NGUYEN[1], SI-PHU LE[1], ANH-TU LE[2], (Student Member, IEEE), NHAN DUC NGUYEN[3], DINH-THUAN DO[4], (Senior Member, IEEE), AND MIROSLAV VOZNAK[1], (Senior Member, IEEE)

[1]Faculty of Electrical Engineering and Computer Science, VSB Technical University of Ostrava, 70800 Ostrava, Czech Republic
[2]Faculty of Electronics Technology, Industrial University of Ho Chi Minh City, Ho Chi Minh 700000, Vietnam
[3]Innovation Center, Van Lang University, Ho Chi Minh 700000, Vietnam
[4]Department of Computer Science and Information Engineering, College of Information and Electrical Engineering, Asia University, Taichung 41354, Taiwan

Corresponding author: Nhan Duc Nguyen (nhan.nd@vlu.edu.vn)

This work was supported by the Ministry of Education, Youth and Sports of the Czech Republic, under Grant SP2021/25 and Grant e-INFRA CZ (ID:90140).

ABSTRACT We investigated the outage performance of non-orthogonal multiple access (NOMA) in satellite-terrestrial systems which contain hardware impairments. An unmanned aerial vehicle (UAV) was implemented to forward signals from a satellite to users on the ground. A two-user model was applied to achieve spectral efficiency. In practical, real-life scenarios, the UAV and ground users encounter issues with imperfect hardware. We examined the performance gap between two users experiencing practical problems such as hardware impairment and imperfect successive interference cancellation (SIC). To implement a practical scenario, Shadow-Rician fading was adopted in the satellite links, and Rician fading was employed in the terrestrial links for ground users. In the main results, we derived the closed-form expression of the outage probability, and to evaluate the system performance of two NOMA users, we obtained the approximate expressions for high signal-to-noise ratios (SNR). Finally, we produced Monte-Carlo simulations to verify the analytical expressions and demonstrate the effect of the main system parameters, such as the number of transmit antennas on the satellite, transmit SNR, and level of hardware impairment on the system performance metric.

INDEX TERMS Non-orthogonal multiple access, satellite-terrestrial systems, outage probability, hardware impairments, UAV.

I. INTRODUCTION

With the development of the fifth generation (5G) network, satellite communications has emerged as a promising technology for application in the 5G ecosystem. Satellite systems may be deployed for reliable connectivity in areas where infrastructure is challenging to establish. To improve spectrum use and serve multiple users in the same time and frequency domains, non-orthogonal multiple access (NOMA) is regarded as one of the technologies which can be applied to address this problem [1]. To minimize masking effects and improve reliability, hybrid satellite-terrestrial relay networks have been implemented as solutions which apply various advances [2]. In [3] and [4], the authors studied outage probability and ergodic capacity and demonstrated the performance of hybrid satellite-terrestrial networks which rely on the amplify-and-forward (AF) relay protocol. To solve the problem of spectrum scarcity, a NOMA system was proposed. NOMA serves multiple users on the same time and frequency resource blocks, improves system capacity, and meets the technical requirements for massive connectivity [5], [6]. In [7]–[9], the authors introduced a NOMA-based satellite system. In [7], NOMA in a downlink mobile satellite network was explored and applied to terrestrial users. They also derived the closed-form expressions for outage probability and ergodic and energy efficiency to validate the effectiveness of proposed system model. In [8], the authors proposed a NOMA cooperative scheme with satellite

The associate editor coordinating the review of this manuscript and approving it for publication was Wei Feng.

communications over a Shadow-Rician fading channel model. One of the main findings was the effect of imperfect successive interference cancellation (ipSIC). The authors of [9] proposed cooperative spectrum sharing in hybrid satellite-terrestrial networks to improve fairness and spectrum use. In that study, the secondary terrestrial network acted as a relay to communicate the primary satellite network. Jain's fairness index was also applied to examine fairness. In [10], the authors presented a cooperative satellite communications system which applies NOMA and introduces a particle swarm optimization algorithm to optimize the system's power allocation factors. A joint iteration algorithm was also proposed to maximize the interference temperature for the satellite in an integrated terrestrial-satellite network-based NOMA [11]. In [12], the authors demonstrated the exact and asymptotic outage probability in a satellite-terrestrial system which relies on cooperative NOMA. In [13], the authors derived the exact analytical expression for the ergodic capacity and outage probability of a satellite-terrestrial system which applies NOMA. In [14], the authors considered the ergodic capacity in a satellite-terrestrial system which uses NOMA.

In [15], the authors introduced cognitive radio (CR) technology as a new technique in satellite communications to enhance spectrum efficiency, referring to the concept as a cognitive satellite-terrestrial network. In [16], the authors defined the interweave, underlay and overlay paradigms as three models of CR. In a CR network, the secondary user (SU) is authorized to share resources with the primary user (PU) provided that the interference caused by the SU is less than a given threshold [17]. Known as a cognitive satellite-terrestrial network, a satellite network which incorporates CR technology is a promising architecture which allows the coexistence of satellite and terrestrial networks in the same frequency band [18]. K. An *et al.* analyzed the exact and asymptotic expressions of the outage probability of a secondary terrestrial mobile network which formed part of a cognitive hybrid satellite-terrestrial network [19]. The authors in [20] and [21] attempted to improve the efficiency of spectral use in CR-based NOMA scenarios in terrestrial networks. In [20], the authors proposed the integration of NOMA with CR into the 5G system, constituting a cognitive NOMA network, for more intelligent spectrum sharing. The authors in [21] introduced a small-cell network based on cognitive hybrid satellite-terrestrial NOMA.

The above-mentioned studies only consider ideal circumstances at the receiver and transmitter, but it is hard to reach such a situation, and in practice, components suffer various types of hardware impairments [22]. Some works have studied the effect of residual hardware impairments (RHIs) on system performance [23], [24]. In [23], a linear channel estimator in the presence of RHIs was proposed. The authors in [24] examined the effect of RHIs on a cooperative full duplex (FD) with NOMA over Rician fading channels. In [25], the effect of RHIs was analyzed on a cognitive network with the presence of interference. In [26], the authors studied the expressions for the outage probability and ergodic capacity for the effect of RHIs on non-cooperative and cooperative NOMA networks. The authors in [27] investigated the effect of hardware impairments (HIs) on two-way multiple relay NOMA-based networks. In [28], a satellite-terrestrial system with single-relay selection and multi-relay selection with RHIs were studied and the expression for outage probability was derived. Unfortunately, the authors did not consider NOMA to improve the spectrum.

The deployment of unmanned aerial vehicles (UAVs) in wireless communications has recently been receiving much attention from researchers and industry in promising applications which cover many areas, for example, civil engineering or military operations [29], [30]. Possessing more advances than current conventional terrestrial infrastructure, UAVs have many advantages over satellite systems, being easier to deploy and having low cost and high mobility.

The authors in [31] developed the application of a UAV in a hybrid satellite-terrestrial network in which a multi-antenna satellite communicates with the ground user equipment (UE). More importantly, this type of system requires the assistance of multiple amplify-and-forward (AF) three-dimensional (3D) mobile UAV relays. The work in [32] replaced AF with decode-and-forward (DF) to evaluate a secure 3D mobile UAV which acts as a relay for a hybrid satellite-terrestrial network. Secure performance must be considered in this case since an aerial eavesdropper would be situated near a serving UAV relay on a circular plane. The study in [33] also explored secure transmission against eavesdroppers by applying a cache-enabled UAV-relaying network assisted with device-to-device (D2D) communications. To prestore the content associated with serving users collaboratively, both the UAVs and D2D users were equipped with cache memory. By simultaneously optimizing transmission power, UAV scheduling and user association, and UAV trajectory, the authors investigated the problem of optimizing the minimum secrecy rate between users to address user fairness. The authors in [34] attained the maximum achievable rate for terrestrial users by simultaneously optimizing transmit power allocation for the base station and UAV trajectory. This system has degraded performance because of the interference temperature threshold imposed by the UAV mobility constraint and satellite network.

The authors in [35] explored 3D channel tracking for a Ka-band UAV-satellite communications system. By considering the probabilistic insight relationship of both the hidden value vector and joint hidden support vector, the authors presented a statistical dynamic channel model which they describe as a 3D two-dimensional Markov model (3D-2D-MM) for a UAV-satellite communications system. The work in [36] proposed enhancing the coverage of a hybrid satellite-terrestrial maritime communications network by employing UAVs. Composite channel models such as large-scale and small-scale fading were adopted. The authors also simultaneously optimized the UAV trajectory and in-flight transmit power subject to the constraints in backhaul, UAV

TABLE 1. Comparison of the proposed system in related works.

Perspective	This work	[8]	[31], [32]	[38]	[39]	[40]
UAV Network	Yes	No	Yes	No	Yes	Yes
NOMA	Yes	Yes	No	Yes	No	Yes
Effect of Hardware Impairments	Yes	No	No	Yes	No	No
Effect of SIC	Yes	Yes	No	No	No	No
Diversity order	Yes	Yes	Yes	Yes	Yes	No
Fading Scenario	Shadow Rician and Rician	Shadow Rician	Shadow Rician and Nakgami-m	Shadow Rician and Rayleigh	Shadow Rician and Nakagami-m	Shadow Rician and Rician

kinematics, tolerable interference and the total energy of the UAV for transmission. The authors in [37] studied a hybrid satellite-terrestrial network which contained imperfect hardware by examining the system's outage probability and corresponding asymptotic outage behavior under an opportunistic relay selection method. This system employs popular channel models, i.e., shadowed Rician channels for the satellite links and Nakagami-*m* and Rician channels for the terrestrial links. Hence, it is important to design a UAV-based satellite system around improvements to the transmissions from the satellite to the users on the ground.

Motivated by the aforementioned studies, we have focused on improving the spectrum efficiency in a UAV-based satellite system network through the application of a NOMA scheme. Specifically, a satellite in geosynchronous orbit (GEO) sends signals to a group of ground users via a UAV. We limited the study to the downlink while the geosynchronous satellite collects and forwards the data generated by ground users. To achieve optimal fairness in the user group, we considered the system performance of a user pair affected by interference from conventional user equipment (CUE). We anticipated that our proposed joint design scheme would exhibit several advantages over the recent studies listed in Table 1. We state two interesting benefits from our considered system: (i) by using the trajectory design, the UAV can be adjusted to fly near each ground user and thereby improve the channel quality and simultaneously move away from the CUE to relieve the effect of interference; (ii) by allocating the different power factors determined by the satellite, the user pair and the different performance at each user can adjusted.

In the present study, we consider the effect of RHI when a mobile UAV assists multi-antenna satellite communications with ground users in the presence of a CUE. Our main contributions in the paper are summarized below:

- We analyze the outage probability as the main system metric in a UAV-assisted satellite system with an opportunistic UAV relay. In contrast to other works on satellite relaying systems, we consider a practical scenario in which the system possesses imperfect hardware. We also consider a realistic deployment case for NOMA users, i.e., CUE is located at a certain fixed distance around NOMA users which have degraded performance due to interference.
- To deploy NOMA, different power allocation factors are assigned to each user, and a corresponding SIC is adopted. It is more meaningful to examine practical circumstances when imperfect SIC (ipSIC) occurs at the UAV and ground users. Together with ipSIC, we aim to evaluate the effects of RHI in the analytical results by determining specific system parameters.
- We also simplify the outage probability expressions to indicate diversity order at asymptotically high SNR to gain insight on the derived system performance metric.

The remainder of the paper is organized as follows: Section II describes the system model and characteristics of the UAV; Section III presents an analysis of the outage probability and performance of different users among a dedicated group of users; Section IV verifies the theoretical results with various numerical simulations; finally, Section V presents conclusions.

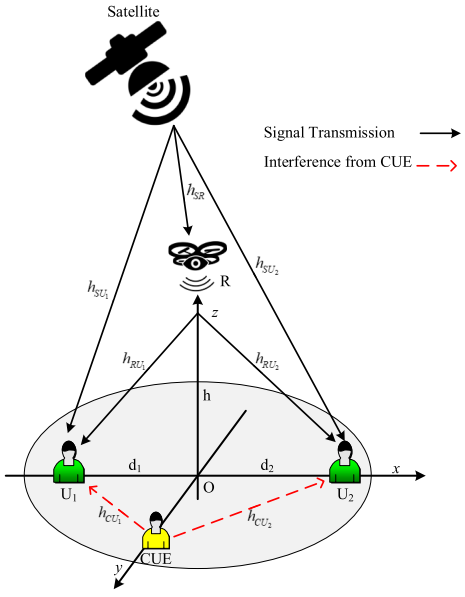

FIGURE 1. Model of an UAV-based satellite-terrestrial system.

II. SYSTEM MODEL

Figure 1 illustrates a UAV-based satellite system which includes a satellite (S), a UAV (R), and two NOMA users $U_i, i \in \{1, 2\}$. In the coverage of the two NOMA users,

TABLE 2. Main notations of the system model.

Symbol	Description
x_i	Signal at U_i
Q_i	Power allocation , where $Q_1 < Q_2$ and $Q_1 + Q_2 = 1$
P_S	Transmit power at S
P_R	Transmit power at R
N	Number of antenna of S
K_i	Rician factor
n_{U_i}, n_{SU_i} and n_R	Additive white Gaussian noise (AWGN), where $n_i \sim CN(0, N_0)$
$CN(\mu, \sigma^2)$	Complex normal distribution with mean μ and variance σ^2
R_i	Target rate
$\|\bullet\|_F$	Frobenius norm
$(\bullet)^\dagger$	Conjugate transpose
χ	Path loss exponent
d_{SR}	Distance from S to UAV
d_{SU_i}	Distance from S to U_i
d_{RU_i}	Distance from UAV to U_i
$\mathbf{h}_{SR}$	Channel vector from satellite to UAV relay
$\mathbf{h}_{SU_i}$	Channel vector from the satellite to the U_i
h_{RU_i}	Channel coefficient from R to U_i
h_{CU_i}	Channel coefficient from CUE to U_i
$\mathrm{E}\{.\}$	Expectation operator
$\Gamma[.;.]$	Upper incomplete gamma function
$\gamma[.;.]$	Lower incomplete gamma function
$\Gamma[.]$	Complete gamma function
$I_i[.]$	First-kind Bessel function with order i

we examine only the worst case of interference from CUE. To improve the strength of the signal transmission, S is assumed to be equipped with N antennas while the remaining nodes R, U_i and CUE are given a simple design and equipped with a single antenna. Due to large separation and heavy shadowing, the direct link from S to the ground users U_i is also assumed unavailable [42]. The main system parameters are presented in Table 2.

Regarding the existence of the UAV, let us consider the three-dimensional Cartesian coordinates (x, y, z) depicted in Figure 1. The UAV relay is located at $R(0, 0, h)$ with altitude h. The locations of ground users U_1 and U_2 are given by the coordinates $U_1(-d_1, 0, 0)$ and $U_2(d_2, 0, 0)$, respectively. From analysis, we can obtain the Euclidean distance from R to U_i according to

$$d_{RU_i} = \sqrt{d_i^2 + h^2}, \tag{1}$$

In the first phase, S sends a signal $\sqrt{P_S}\left(\sqrt{Q_1}x_1 + \sqrt{Q_2}x_2\right)$ to the UAV (node R) and U_i. The signals received at the UAV and U_i are respectively given as

$$\begin{aligned} y_R = &\sqrt{L_{SR}\vartheta_S\vartheta\left(\phi_R\right)}\mathbf{h}_{SR}^\dagger\mathbf{h}_{SR} \\ &\times\left(\sqrt{P_S}\left(\sqrt{Q_1}x_1 + \sqrt{Q_2}x_2\right) + \eta_R\right) + n_R, \end{aligned} \tag{2}$$

$$\begin{aligned} y_{SU_i} = &\sqrt{L_{SU_i}\vartheta_S\vartheta\left(\phi_{U_i}\right)}\mathbf{h}_{SU_i}^\dagger\mathbf{h}_{SU_i} \\ &\times\left(\sqrt{P_S}\left(\sqrt{Q_1}x_1 + \sqrt{Q_2}x_2\right) + \eta_{SU_i}\right) \\ &+ P_{CUE}h_{CU_i} + n_{U_i}, \end{aligned} \tag{3}$$

where ϑ_S is the satellite antenna gain, η_R and η_{SU_i} are the distortion noises caused by RHI where $\eta_R \sim CN\left(0, \kappa_R^2 P_S\right)$ and $\eta_{SU_i} \sim CN\left(0, \kappa_{SU_i}^2 P_S\right)$ and κ_R and κ_{SU_i} are the levels of hardware impairment associated with the link from S to R and S to U_i, respectively [25]. We denote $\mathbf{w}_i$ as the weight vector and apply the maximum ratio transmission [46], $\mathbf{w}_{Sj} = \frac{\mathbf{h}_{SR}}{\|\mathbf{h}_{Sj}\|_F}$ for $j \in \{R, U_1, U_2\}$. In addition, $L_{SR} = \frac{1}{K_B TW}\left(\frac{c}{4\pi f_c d_{SR}}\right)^2$ and $L_{SU_i} = \frac{1}{K_B TW}\left(\frac{c}{4\pi f_c d_{SU_i}}\right)^2$ denote the instantaneous free space loss [39], where $K_B = 1.38\times10^{-23}J/K$ is the Boltzman constant, W and T are the carrier bandwidth and receiver noise temperature, respectively, c represents the speed of light, and f_c is the carrier frequency.

To characterize the link from S to R and S to U_i, $\vartheta\left(\phi_j\right)$ represents the beam gain and is expressed by

$$\vartheta\left(\phi_j\right) = \vartheta_j\left(\frac{I_1\left(\bar{\rho}_j\right)}{2\rho_j} + 36\frac{I_3\left(\bar{\rho}_j\right)}{\rho_j^3}\right), \tag{4}$$

where ϑ_R and ϑ_{U_i} are the antenna gains at the UAV and U_i, respectively, ϕ_j is the angular separation, $\bar{\rho}_j = 2.07123\frac{\sin\phi_j}{\sin\phi_{R3\mathrm{dB}}}$, and $\phi_{R3\mathrm{dB}}$ represents 3dB beamwidth [39].

In the first phase, the signals for the link from S to R and R to D_i are processed, and to detect the signals as expected, the signal to interference plus noise ratio (SINR) is determined.

The SINR at U_2 to detect x_2 is given by (5), which is shown at the bottom of the page.

Then, the SINR at U_1 to detect x_2 is given by

$$\gamma_{SU_1}^{x_2} = \frac{\beta_{SU_1}Q_2}{\beta_{SU_1}Q_1 + \beta_{SU_1}\kappa_{SU_1}^2 + \rho_{CU}\left|h_{CU_1}\right|^2 + 1}, \tag{6}$$

where $\rho_S = \frac{P_S}{N_0}$, $\rho_{CU} = \frac{P_{CUE}}{N_0}$, $\rho_{Sj} = \rho_S L_{Sj}\vartheta_S\vartheta\left(\phi_j\right)$ and $\beta_{Sj} = \rho_{Sj}\left\|\mathbf{h}_{Sj}\right\|_F^2$. Then, by performing SIC to eliminate x_2, treating signal x_2 as a noise term, x_1 is detected at the UAV. To do this, we compute the SINR from

$$\gamma_{SU_1}^{x_1} = \frac{\beta_{SU_1}Q_1}{\rho_{SU_1}|g|^2 + \beta_{SU_1}\kappa_{SU_1}^2 + \rho_{CU}\left|h_{CU_1}\right|^2 + 1}. \tag{7}$$

Due to the effect of ipSIC, g is an interference channel modeled as a Rayleigh fading channel where $g \sim CN(0, \lambda_g)$ [8].

$$\begin{aligned} \gamma_{SU_2}^{x_2} &= \frac{P_S L_{SU_2}\vartheta\left(\phi_{U_2}\right)Q_2\left\|h_{SU_2}\right\|_F^2}{P_S L_{SU_2}\vartheta\left(\phi_{U_2}\right)Q_1\left\|h_{SU_2}\right\|_F^2 + P_S L_{SU_2}\vartheta\left(\phi_{U_2}\right)\|h_{SR}\|_F^2\kappa_{SU_2}^2 + P_{CUE}\left\|h_{CU_2}\right|^2 + N_0} \\ &= \frac{\beta_{SU_2}Q_2}{\beta_{SU_2}Q_1 + \beta_{SU_2}\kappa_{SU_2}^2 + \rho_{CU}\left|h_{CU_2}\right|^2 + 1}. \end{aligned} \tag{5}$$

Similarly, the SINR at the UAV to detect x_2 is given as

$$\gamma_{SR}^{x_2} = \frac{\beta_{SR} Q_2}{\beta_{SR} Q_1 + \beta_{SR}\kappa_R^2 + 1}. \quad (8)$$

Applying SIC to detect signal x_1, the SINR is given as

$$\gamma_{SR}^{x_1} = \frac{\beta_{SR} Q_1}{\rho_{SR} |g|^2 + \beta_{SR}\kappa_R^2 + 1}. \quad (9)$$

In the second phase, the UAV sends the signal to two NOMA users. The signal received at U_i is given as

$$y_{RU_i} = \sqrt{\frac{P_S}{d_{RU_i}^{\chi}}} h_{RU_i} \left(\left(\sqrt{Q_1} x_1 + \sqrt{Q_2} x_2 \right) + \eta_{U_i} \right) + P_{CUE} h_{CU_i} + n_{RU_i}, \quad (10)$$

where η_{U_i} is the distortion noise caused by RHIs for $\eta_{U_i} \sim CN\left(0, \kappa_i^2 P_R\right)$, κ_i is the level of hardware impairments from R to U_i, h_{CU_i} is the channel from CUE following a Rayleigh fading channel with $\mathrm{E}\{h_{CU_i}\} = 1$

The SINR at U_2 to detect the signal x_2 is given as

$$\gamma_{RU_2}^{x_2} = \frac{P_R Q_2 \left|h_{RU_2}\right|^2}{P_R Q_1 \left|h_{RU_2}\right|^2 + P_R \left|h_{RU_2}\right|^2 \kappa_2^2 + P_{CUE} \left|h_{CU_2}\right|^2 + N_0} = \frac{\beta_{RU_2} Q_2}{\beta_{RU_2} Q_1 + \beta_{RU_2}\kappa_2^2 + \rho_{CU} \left|h_{CU_2}\right|^2 + 1}, \quad (11)$$

where $\rho_R = \frac{P_R}{N_0}$, $\rho_{CU} = \frac{P_{CUE}}{N_0}$, $\rho_{RU_i} = \frac{\rho_R}{d_{RU_i}^{\chi}}$ and $\beta_{RU_i} = \rho_{RU_i} \left|h_{RU_i}\right|^2$. Then, the SINR at U_1 to detect signal x_2 is given as

$$\gamma_{RU_1}^{x_2} = \frac{\beta_{RU_1} Q_2}{\beta_{RU_1} Q_1 + \beta_{RU_1}\kappa_1^2 + \rho_{CU} \left|h_{CU_1}\right|^2 + 1}. \quad (12)$$

The SINR at U_1 to detect it's the own signal x_1 is given as

$$\gamma_{RU_1}^{x_1} = \frac{\beta_{RU_1} Q_1}{\rho_{RU_1} |g|^2 + \beta_{RU_1}\kappa_1^2 + \rho_{CU} \left|h_{CU_1}\right|^2 + 1}. \quad (13)$$

Remark 1: These SINR expressions are crucial in evaluating other main system metrics and provide a guide to implementing a UAV-based satellite system in practical scenarios. We can observe in the SINR equations, for example (11), (12), *and* (13), *the corresponding SINRs are determined by the channel gains, the power allocation factors Q_1 and Q_2, and the levels of RHI. In addition, the transmit power at the satellite and the UAV play other roles in improving system performance. We consider these effects in the following section.*

III. OUTAGE PROBABILITY ANALYSIS

A. CHANNEL CHARACTERIZATION

To further compute the system performance metric, let us assume that the channel coefficients are independent and identically distributed (i.i.d.). Then, the probability density function (PDF) of the channel coefficient $h_{Sj}^{(j)}$ from the satellite's q-th antenna to the UAV is expressed as [44]

$$f_{\left|h_{Sj}^{(q)}\right|^2}(\gamma) = e^{-\varepsilon_{SR}\gamma} \alpha_{Sj} {}_1F_1\left(m_{SR}; 1; \delta_{SR}\gamma\right), \quad (14)$$

where $\varepsilon_{Sj} = \frac{1}{2b_{Sj}}$, $\alpha_{SR} = \frac{1}{2b_{Sj}} \left(\frac{2b_{Sj} m_{Sj}}{2b_{Sj} m_{Sj} + \Omega_{Sj}} \right)^{m_{Sj}}$, $\delta_{Sj} = \frac{\Omega_{Sj}}{2b_{Sj}(2b_{Sj} m_{Sj} + \Omega_{Sj})}$, and where Ω_{Sj}, $2b_{Sj}$ and m_{Sj} are the average powers of LOS, the multipath components and the fading severity parameter, respectively. ${}_1F_1(.;.;.)$ denotes a confluent hypergeometric function of the first kind [47, eq. 9.210]. Then, we assume the integer values of the Shadowed-Rician fading severity parameter throughout this paper. We can rewrite (14) as

$$f_{\left|h_{Sj}^{(q)}\right|^2}(\gamma) = e^{-\Delta_{SR}\gamma} \alpha_{SR} \sum_{b=0}^{m_{Sj}-1} \zeta_{Sj}(b) \gamma^b, \quad (15)$$

where $\Delta_{Sj} = \varepsilon_{Sj} - \delta_{Sj}$, $\zeta_{Sj}(z) = \frac{(-1)^z (1-m_{Sj})_z (\delta_{Sj})^z}{(z!)^2}$, and $(.)_x$ is the Pochhammer symbol [47, p.xliii]. Applying the result from [3], the PDF of $\left\|\mathbf{h}_{Sj}\right\|_F^2$ under i.i.d. Shadowed-Rician fading can be formulated as

$$f_{\|\mathbf{h}_{Sj}\|_F^2}(x) = \sum_{b_1=0}^{m_{Sj}-1} \cdots \sum_{b_N=0}^{m_{Sj}-1} \Xi(Sj) \gamma^{\Lambda-1} e^{-\Delta_{Sj}\gamma}, \quad (16)$$

where

$$\Xi(Sj) = \alpha_{Sj}^N \prod_{u=1}^{N} \zeta_{Sj}(b_u) \prod_{v=1}^{N-1} B\left(\sum_{l=1}^{v} b_l + v, b_{v+1} + 1 \right), \quad (17)$$

$$\Lambda = \sum_{u=1}^{N} b_u + N. \quad (18)$$

and $B(.,.)$ is the Beta function [47, eq. 8.384.1]. From the above analysis, the PDF of β_{Sj} is expressed as

$$f_{\beta_{Sj}}(\gamma) = \sum_{b_1=0}^{m_{Sj}-1} \cdots \sum_{b_N=0}^{m_{Sj}-1} \frac{\Xi(Sj)}{\left(\rho_{Sj}\right)^{\Lambda}} \gamma^{\Lambda-1} e^{-\frac{\Delta_{Sj}}{\rho_{Sj}}\gamma}. \quad (19)$$

Using [47, eq. 3.351.1], we obtain the CDF of β_{Sj} as

$$F_{\beta_{Sj}}(\gamma) = \sum_{b_1=0}^{m_{Sj}-1} \cdots \sum_{b_N=0}^{m_{Sj}-1} \frac{\Xi(Sj)}{\left(\Delta_{Sj}\right)^{\Lambda}} \gamma\left(\Lambda, \frac{\Delta_{Sj}}{\rho_{Sj}}\gamma\right). \quad (20)$$

Then, the PDF of the links from R to U_i can be expressed as [40]

$$f_{|h_{RU_i}|^2}(\gamma) = \varpi_i e^{-K_i} e^{-\varpi_i \gamma} I_0\left(2\sqrt{\varpi_i K_i \gamma}\right), \quad (21)$$

where $\varpi_i = \frac{(1+K_i)}{\Omega_i}$, and K_i and Ω_i are the Rician factor and average fading power, respectively. Then, the PDF of β_{RU_i} can be expressed as

$$f_{\beta_{RU_i}}(\gamma) = \frac{\varpi_i e^{-K_i}}{\rho_{RU_i}} e^{-\frac{\varpi_i}{\Omega_i}\gamma} I_0\left(2\sqrt{\frac{K_i \varpi_i}{\rho_{RU_i}}\gamma}\right). \quad (22)$$

Based on [47, eq. 8447.1], we can then rewrite

$$f_{\beta_{RU_i}}(\gamma) = \sum_{b=0}^{\infty} \frac{(K_i)^b e^{-K_i}}{(b!)^2} \left(\frac{\varpi_i}{\rho_{RU_i}}\right)^{b+1} \gamma^b e^{-\frac{\varpi_i}{\rho_{RU_i}}\gamma}. \quad (23)$$

Similarly, the CDF of β_{RU_i} can be expressed as

$$F_{\beta_{RU_i}}(\gamma) = \sum_{b=0}^{\infty} \frac{(K_i)^b e^{-K_i}}{(b!)^2} \gamma\left(b+1, \frac{\varpi_i}{\rho_{RU_i}}\gamma\right). \quad (24)$$

B. OUTAGE PROBABILITY OF U_1

The outage probability defines that the probability of the instantaneous SINR γ_k falls below a predefined threshold φ_{th}, i.e.,

$$P_{out} = \Pr(\gamma_k < \varphi_{th}), \quad (25)$$

where Pr(.) is the probability function.

Based on the selection combining technique, the outage probability of U_1 can be determined by maximizing the SINR of the link from S to U_i and the link from S to R. The outage probability of U_1 can then be expressed as [41]

$$P_{out,1} = \Psi_1 \times \Psi_2, \quad (26)$$

where

$$\Psi_1 = 1 - \Pr\left(\gamma_{SU_1}^{x_2} > \varphi_2, \gamma_{SU_1}^{x_1} > \varphi_1\right), \quad (27)$$

$$\Psi_2 = 1 - \Pr\left(\gamma_{SR}^{x_2} > \varphi_2, \gamma_{SR}^{x_1} > \varphi_1\right) \times \Pr\left(\gamma_{SR}^{x_2} > \varphi_2, \gamma_{SR}^{x_1} > \varphi_1\right), \quad (28)$$

and where $\varphi_i = 2^{R_i} - 1$, R_i are the target rates.

Lemma 1: The term Ψ_1 is given as

$$\Psi_1 = 1 - I_1 + I_2, \quad (29)$$

where I_1 and I_2 are expressed by

$$I_1 = \sum_{b_1=0}^{m_{SU_1}-1} \cdots \sum_{b_N=0}^{m_{SU_1}-1} \sum_{a=0}^{\Lambda-1} \frac{\Xi(SU_1)\,\Gamma(\Lambda)\, e^{-\frac{\Delta_{SU_1}\upsilon_{\max}}{\rho_{SU_1}}}}{a!\lambda_{CU_1}\left(\Delta_{SU_1}\right)^{\Lambda-a}} \times \left(\frac{\upsilon_{\max}}{\rho_{CU}\rho_{SU_1}}\right)^a \left(\frac{1}{\lambda_{CU_1}} + \frac{\Delta_{SU_1}\upsilon_{\max}\rho_{CU}}{\rho_{SU_1}}\right)^{-a-1} \times e^{\frac{1}{\lambda_{CU_1}\rho_{CU}} + \frac{\Delta_{SU_1}\upsilon_{\max}}{\rho_{SU_1}}} \Gamma\left(a+1, \frac{1}{\lambda_{CU_1}\rho_{CU}} + \frac{\Delta_{SU_1}\upsilon_{\max}}{\rho_{SU_1}}\right), \quad (30)$$

and

$$I_2 = \sum_{b_1=0}^{m_{SU_1}-1} \cdots \sum_{b_N=0}^{m_{SU_1}-1} \Xi(SU_1) \sum_{a=0}^{\Lambda-1} \frac{(\Lambda-1)!\,(\upsilon_{\max})^a\, e^{-\Theta_2}}{\lambda_{CU_1} a!\,(\Theta_1)^{a+1}} \times \left(\Delta_{SU_1} + \frac{1}{\upsilon_1\lambda_g}\right)^{-\Lambda+a} \left(\frac{\rho_{CU}}{\rho_{SU_1}}\right)^a e^{\frac{\Theta_1}{\rho_{CU}}} \Gamma\left(a+1, \frac{\Theta_1}{\rho_{CU}}\right). \quad (31)$$

Proof: See Appendix A.

Lemma 2: The closed-form expression to compute Ψ_2 can be expressed as

$$\Psi_2 = 1 - A_1 \times A_2. \quad (32)$$

Because the computations of A_1 and A_2 are complicated, we present these details in the appendix.

Proof: See Appendix B

C. OUTAGE PROBABILITY OF U_2

Similarly, the outage probability of U_2 is given as [41]

$$P_{out,2} = \bar{\Psi}_1 \times \bar{\Psi}_2, \quad (33)$$

where

$$\bar{\Psi}_1 = 1 - \Pr\left(\gamma_{SU_2}^{x_2} > \varphi_2\right) \quad (34)$$

and

$$\bar{\Psi}_2 = 1 - \Pr\left(\gamma_{SR}^{x_2} > \varphi_2, \gamma_{SR}^{x_1} > \varphi_1\right) \Pr\left(\gamma_{RU_2}^{x_2} > \varphi_2\right). \quad (35)$$

Lemma 3: The closed-form expression of the outage probability, denoted by $\bar{\Psi}_1$, is given as

$$\bar{\Psi}_1 = 1 - \sum_{b_1=0}^{m_{SU_2}-1} \cdots \sum_{b_N=0}^{m_{SU_2}-1} \frac{\Xi(SU_2)\,(\rho_{CU}\upsilon_2)^a\, e^{-\frac{\Delta_{SU_2}\upsilon_2}{\rho_{SU_2}}}}{\left(\rho_{SU_2}\right)^a \lambda_{CU_2}\left(\Delta_{SU_2}\right)^{\Lambda-a}} \times \sum_{a=0}^{\Lambda-1} \frac{(\Lambda-1)!}{a!}\Gamma\left(a+1, \frac{1}{\lambda_{CU_2}\rho_{CU}} + \frac{\Delta_{SU_2}\rho_{CU}\upsilon_2}{\rho_{SU_2}\rho_{CU}}\right) \times \left(\frac{1}{\lambda_{CU_2}} + \frac{\Delta_{SU_2}\rho_{CU}\upsilon_2}{\rho_{SU_2}}\right)^{-a-1} e^{\frac{1}{\lambda_{CU_2}\rho_{CU}} + \frac{\Delta_{SU_2}\rho_{CU}\upsilon_2}{\rho_{SU_2}\rho_{CU}}}. \quad (36)$$

Proof: From the result from (5), we can rewrite (36) as

$$\bar{\Psi}_1 = 1 - \Pr\left(\beta_{SU_2} > \upsilon_2\left(\rho_{CU}\left|h_{CU_2}\right|^2 + 1\right)\right) = 1 - \int_0^{\infty} f_{|h_{CU_2}|^2}(y) \int_{\upsilon_2(\rho_{CU}y+1)}^{\infty} f_{\beta_{SU_2}}(x)\,dx\,dy. \quad (37)$$

Then, we calculate

$$\bar{\Psi}_1 = 1 - \sum_{b_1=0}^{m_{SU_2}-1} \cdots \sum_{b_N=0}^{m_{SU_2}-1} \frac{\Xi(SU_2)}{\left(\rho_{SU_2}\right)^{\Lambda}\lambda_{CU_2}} \times \int_0^{\infty} e^{-\frac{y}{\lambda_{CU_2}}} \int_{\upsilon_2(\rho_{CU}y+1)}^{\infty} x^{\Lambda-1} e^{-\frac{\Delta_{SU_2}}{\rho_{SU_2}}x}\,dx\,dy. \quad (38)$$

Next, $\bar{\Psi}_1$ can then be expressed as

$$\bar{\Psi}_1 = 1 - \sum_{b_1=0}^{m_{SU_2}-1} \cdots \sum_{b_N=0}^{m_{SU_2}-1} \frac{\Xi(SU_2)\, e^{-\frac{\Delta_{SU_2}\upsilon_2}{\rho_{SU_2}}}}{\left(\rho_{SU_2}\right)^a \lambda_{CU_2}} \times \sum_{a=0}^{\Lambda-1} \frac{(\Lambda-1)!\,(\rho_{CU}\upsilon_2)^a}{a!\left(\Delta_{SU_2}\right)^{\Lambda-a}} \times \int_0^{\infty} \left(y + \frac{1}{\rho_{CU}}\right)^a e^{-\left(\frac{1}{\lambda_{CU_2}} + \frac{\Delta_{SU_2}\rho_{CU}\upsilon_2}{\rho_{SU_2}}\right)y} dy. \quad (39)$$

We thus similarly obtain $\bar{\Psi}_1$. This ends the proof.

Lemma 4: The term $A_3 = \Pr\left(\gamma_{RU_2}^{x_2} > \varphi_2\right)$ can be expressed as

$$A_3 = \sum_{b=0}^{\infty} \sum_{c=0}^{b} \frac{(K_2)^b\, \rho_{RU_2} e^{-K_2} \left(\tilde{\theta}_2\varpi_2\rho_{CU}\lambda_{CU_2}\right)^c}{b!c!\left(\tilde{\theta}_2\varpi_2\lambda_{CU_2}\rho_{CU} + \rho_{RU_2}\right)^{c+1}}$$

$$\times e^{-\frac{\tilde{\theta}_2\varpi_2}{\rho_{RU_2}}+\frac{\tilde{\theta}_2\varpi_2\lambda_{CU_2}\rho_{CU}+\rho_{RU_2}}{\lambda_{CU_2}\rho_{CU}\rho_{RU_2}}}$$
$$\times\Gamma\left(c+1,\frac{\tilde{\theta}_2\varpi_2\lambda_{CU_2}\rho_{CU}+\rho_{RU_2}}{\lambda_{CU_2}\rho_{CU}\rho_{RU_2}}\right). \quad (40)$$

Proof: Applying (11), A_3 can be expressed as

$$A_3=\Pr\left(\beta_{RU_2}>\tilde{\theta}_2\left(\rho_{CU}\left|h_{CU_2}\right|^2+1\right)\right)$$
$$=\int_0^{\infty}\int_{\tilde{\theta}_2(\rho_{CU}x+1)}^{\infty} f_{|h_{CU_2}|^2}(x)f_{\beta_{RU_2}}(y)dydx. \quad (41)$$

Similarly, (41) can be expressed as

$$A_3=\sum_{b=0}^{\infty}\sum_{c=0}^{b}\frac{(K_2)^b e^{-K_2}}{b!c!\lambda_{CU_2}}e^{-\frac{\varpi_1\tilde{\theta}_2}{\rho_{RU_1}}}\left(\frac{\tilde{\theta}_2\rho_{CU}\varpi_2}{\rho_{RU_2}}\right)^c$$
$$\times\int_0^{\infty}\left(x+\frac{1}{\rho_{CU}}\right)^c e^{-\frac{\varpi_2\tilde{\theta}_2\rho_{CU}}{\rho_{RU_2}}x-\frac{x}{\lambda_{CU_2}}}dydx. \quad (42)$$

We thus obtain (14) similarly to (60). This ends the proof.

Finally, by combining (29) and (40), the closed-form expression of the outage probability, i.e., $\bar{\Psi}_2$, is expressed by

$$\bar{\Psi}_2=1-A_1\times A_3. \quad (43)$$

Remark 2: The expressions for outage probability depend on various system parameters determined from the constraints encountered in practical scenarios. We can observe in the relevant outage probability equations, for example (27) *and* (33)*, the effects due to the number of transmit antennas at the satellite, the satellite link configuration, the satellite transmit power, the power allocation factors Q_1 and Q_2, and the levels of RHI. Applying numerical simulations, we verify these effects in the system performance metrics.*

D. DIVERSITY ORDER

To provide more insight, we need to derive an asymptotic expression of the outage probability at a high SNR $\rho=\rho_S=\rho_R\to\infty$. The diversity order of the terrestrial user can be given by [43]

$$d=-\lim_{\rho\to\infty}\frac{\log\left(P_{out}^{\infty}(\rho)\right)}{\log\rho}, \quad (44)$$

where P_{out}^{∞} denotes the asymptotic outage probability.

Then, by applying a Maclaurin series, we have $e^{-x}\simeq(1-x)$. We can also write (26) in the case of a high SNR as

$$P_{out,1}^{\infty}=\Psi_1^{\infty}\times\Psi_2^{\infty}, \quad (45)$$

where Ψ_1^{∞} is expressed as

$$\Psi_1^{\infty}=1-\sum_{b_1=0}^{m_{SU_1}-1}\cdots\sum_{b_N=0}^{m_{SU_1}-1}\sum_{a=0}^{\Lambda-1}\sum_{b=0}^{a}\frac{\Xi(SU_1)\Gamma(\Lambda)}{b!\lambda_{CU_1}\left(\Delta_{SU_1}\right)^{\Lambda-a}}$$
$$\times\left(1-\frac{\Delta_{SU_1}\theta_{\max}}{\rho_{SU_1}}\right)\left(\frac{1}{\lambda_{CU_1}}+\frac{\Delta_{SU_1}\theta_{\max}\rho_{CU}}{\rho_{SU_1}}\right)^{-a-1}$$
$$\times\left(\frac{\theta_{\max}}{\rho_{CU}\rho_{SU_1}}\right)^a\left(\frac{1}{\lambda_{CU_1}\rho_{CU}}+\frac{\Delta_{SU_1}\theta_{\max}}{\rho_{SU_1}}\right)^b$$
$$+\sum_{b_1=0}^{m_{SU_1}-1}\cdots\sum_{b_N=0}^{m_{SU_1}-1}\sum_{a=0}^{\Lambda-1}\sum_{b=0}^{a}\frac{\Xi(SU_1)\Gamma(\Lambda)(1-\Theta_2)}{\lambda_{CU_1}b!(\Theta_1)^{a+1}}$$
$$\times\left(\frac{\upsilon_{\max}\rho_{CU}}{\rho_{SU_1}}\right)^a\left(\frac{\Theta_1}{\rho_{CU}}\right)^b\left(\Delta_{SU_1}+\frac{1}{\upsilon_1\lambda_g}\right)^{-\Lambda+a}. \quad (46)$$

Then, Ψ_1^{∞} is given by

$$\Psi_1^{\infty}=1-A_1^{\infty}\times A_2^{\infty}, \quad (47)$$

where

$$A_1^{\infty}=\sum_{b_1=0}^{m_{SR}-1}\cdots\sum_{b_N=0}^{m_{SR}-1}\Xi(SR)\sum_{n=0}^{\Lambda-1}\frac{(\Lambda-1)!}{n!(\Delta_{SR})^{\Lambda}}$$
$$\times\left(1-\frac{\Delta_{SR}\theta_{\max}}{\rho_{SR}}\right)\left(\frac{\Delta_{SR}\theta_{\max}}{\rho_{SR}}\right)^n$$
$$-\sum_{b_1=0}^{m_{SR}-1}\cdots\sum_{b_N=0}^{m_{SR}-1}\Xi(SR)\sum_{n=0}^{\Lambda-1}\frac{(\Lambda-1)!}{n!}$$
$$\times\left(\frac{\theta_1\lambda_g}{\Delta_{SR}\lambda_g\theta_1+1}\right)^{\Lambda-n}\left(\frac{\theta_{\max}}{\rho_{SR}}\right)^n$$
$$\times\left(1-\frac{\left(\Delta_{SR}\lambda_g\theta_1+1\right)\theta_{\max}}{\theta_1\rho_{SR}\lambda_g}+\frac{1}{\rho_{SR}\lambda_g}\right), \quad (48)$$

and

$$A_2^{\infty}=\sum_{b=0}^{\infty}\sum_{c=0}^{b}\sum_{d=0}^{c}\frac{(K_1)^b e^{-K_1}\rho_{RU_1}}{d!b!\lambda_{CU_1}}$$
$$\times\frac{\left(\varpi_1\tilde{\theta}_{\max}\rho_{CU}\lambda_{CU_1}\right)^c}{\left(\varpi_1\tilde{\theta}_{\max}\rho_{CU}\lambda_{CU_1}+\rho_{RU_1}\right)^{c+1}}$$
$$\times\left(\frac{\varpi_1\tilde{\theta}_{\max}\rho_{CU}\lambda_{CU_1}+\rho_{RU_1}}{\rho_{RU_1}\rho_{CU}\lambda_{CU_1}}\right)^d\left(1-\frac{\varpi_1\tilde{\theta}_{\max}}{\rho_{RU_1}}\right)$$
$$-\sum_{b=0}^{\infty}\sum_{c=0}^{b}\sum_{d=0}^{c}\frac{(K_1)^b(\varpi_1)^{b+1}e^{-K_1}}{d!c!\lambda_{CU_1}\xi^{c+1}}$$
$$\times\left(\frac{\lambda_g\tilde{\theta}_1}{\varpi_1\lambda_g\tilde{\theta}_1+1}\right)^{b-c+1}\left(\frac{\rho_{CU}\tilde{\theta}_{\max}}{\rho_{RU_1}}\right)^c\left(\frac{\xi}{\rho_{CU}}\right)^d$$
$$\times\left(1-\frac{\left(\varpi_1\lambda_g\tilde{\theta}_1+1\right)\tilde{\theta}_{\max}}{\lambda_g\tilde{\theta}_1\rho_{RU_1}}+\frac{1}{\lambda_g\rho_{RU_1}}\right). \quad (49)$$

The asymptotic outage probability for U_2 is thus similarly obtained as

$$P_{out,2}^{\infty}=\bar{\Psi}_1\times\bar{\Psi}_2, \quad (50)$$

where $\bar{\Psi}_1$ is given by

$$\bar{\Psi}_1^{\infty}=1-\sum_{b_1=0}^{m_{SU_2}-1}\cdots\sum_{b_N=0}^{m_{SU_2}-1}\frac{\Xi(SU_2)(\rho_{CU}\upsilon_2)^a}{\left(\rho_{SU_2}\right)^a\left(\Delta_{SU_2}\right)^{\Lambda-a}}$$

TABLE 3. Table of satellite channel parameters [45].

Shadowing	b	m	Ω
Average shadowing (AS)	0.251	5	0.279
Heavy shadowing (HS)	0.063	1	0.0007

TABLE 4. Table of main simulated parameters.

Monte Carlo simulations	10^6 iterations
Satellite type	GEO
Carrier frequency	$f_c = 2GHz$
Carrier bandwidth	$W = 15Mhz$
Distance from satellite to UAV and satellite to U_i	$d_{SR} = d_{SU_1} = d_{SU_2} = 35786Km$
Receiver noise temperature	$T = 500^oK$
Speed of light	$c = 3\times10^8 m/s$
Antenna gain at satellite	$\vartheta_S = 4$dBi
Antenna gain at UAV and U_i	$\vartheta_R = \vartheta_{U_i} = 48$dB
Angular separation	$\phi_R = 0.8^o$
3dB beamwidth	$\phi_{R3dB} = 0.3^o$
Power allocation	$Q_1 = 0.25$ and $Q_2 = 0.75$
Path loss exponent	$\chi = 2$
Level of hardware impairment	$\kappa^2 = \kappa^2_{SU_i} = \kappa^2_R = \kappa^2_i = 0.01$
Altitude	$h = 10$m
Target rate	$R_1 = 0.2$ (BPCU) and $R_2 = 0.4$ (BPCU)
Rician factor	$K_1 = K_2 = 5$
Average fading power	$\Omega_1 = \Omega_2 = 1$
Distance	$d_1 = 5$m and $d_2 = 10$m

$$\times \sum_{a=0}^{\Lambda-1}\sum_{b=0}^{a}\frac{(\Lambda-1)!}{b!\lambda_{CU_2}}\left(\frac{1}{\lambda_{CU_2}}+\frac{\Delta_{SU_2}\rho_{CU}\upsilon_2}{\rho_{SU_2}}\right)^{-a-1}$$
$$\times\left(\frac{1}{\lambda_{CU_2}\rho_{CU}}+\frac{\Delta_{SU_2}\rho_{CU}\upsilon_2}{\rho_{SU_2}\rho_{CU}}\right)^{a}$$
$$\times\left(1+\frac{1}{\lambda_{CU_2}\rho_{CU}}+\frac{\Delta_{SU_2}\rho_{CU}\upsilon_2}{\rho_{SU_2}\rho_{CU}}\right)$$
$$\times\left(1-\frac{1}{\lambda_{CU_2}\rho_{CU}}-\frac{\Delta_{SU_2}\rho_{CU}\upsilon_2}{\rho_{SU_2}\rho_{CU}}-\frac{\Delta_{SU_2}\upsilon_2}{\rho_{SU_2}}\right). \quad (51)$$

Then, $\bar{\Psi}_2$ is given by

$$\bar{\Psi}_2 = 1-A_1^{\infty}\times A_3^{\infty}, \quad (52)$$

where

$$A_3^{\infty} = \sum_{b=0}^{\infty}\sum_{c=0}^{b}\sum_{d=0}^{c}\frac{(K_2)^b\,\rho_{RU_2}e^{-K_2}\left(\tilde{\theta}_2\varpi_2\rho_{CU}\lambda_{CU_2}\right)^c}{b!d!\left(\tilde{\theta}_2\varpi_2\lambda_{CU_2}\rho_{CU}+\rho_{RU_2}\right)^{c+1}}$$
$$\times\left(1-\frac{\tilde{\theta}_2\varpi_2}{\rho_{RU_2}}\right)\left(\frac{\tilde{\theta}_2\varpi_2\lambda_{CU_2}\rho_{CU}+\rho_{RU_2}}{\lambda_{CU_2}\rho_{CU}\rho_{RU_2}}\right)^d. \quad (53)$$

We may straightforwardly conclude that the diversity orders of users U_1 and U_2 both equal zero.

IV. NUMERICAL RESULTS

In this section, we present numerical simulations to verify the derived expressions. The Shadowed-Rician fading parameters are listed in Table 3, and the parameters for the numerical results are summarized in Table 4, where BPCU refers to *bit per channel use*. We also set $\rho = \rho_S = \rho_R$, with the exception of the specific case mentioned later.

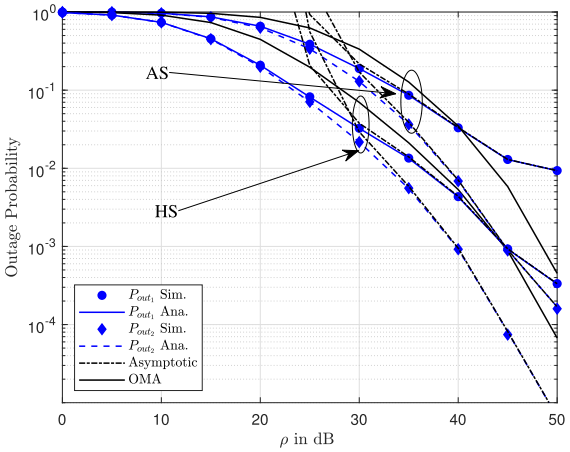

FIGURE 2. Outage probability versus ρ for different values of the satellite link, where $N = 1$, $\rho_{CU} = 15$dB, and $\lambda_g = 0.01$.

Figure 2 depicts the outage performance of the UAV-based satellite system against the transmit SNR at the satellite ρ. From the illustration, we can see that the outage probability decreases for two users as the value of ρ increases. A clear observation is that the performance gap between two users is just as large at the middle range of the SNR, i.e., ρ varies from 40 to 50 (dB). This is significant because we can see that the Monte-Carlo and analytical simulations match very closely, confirming the corrections in the related expressions for outage probability. The asymptotic curves match with exact curves in the high SNR region, verifying the validity of the corresponding expressions. The advantage of the proposed system is clear in a comparison of its performance with an OMA-assisted satellite-terrestrial system. By adjusting the power allocation factors (Q_1, and Q_2), the system can also produce different performance for two users, however, in the high SNR region, the system performance does not depend on Q_1 and Q_2. The configuration of AS mode is superior to that of HS, and outage performance for both users therefore improves when the satellite links are subject to AS rather than HS.

Figure 3 shows the improvement of outage performance at high SNR. When we increase ρ, the corresponding outage performance of two users improves significantly, especially if we raise the number of transmit antennas at the satellite from $N = 1$ to $N = 2$ or $N = 3$. For $N = 3$, we obtained better results. A greater number of antennas equipped at the satellite improves the channel gain, which results in better performance, especially in the performance gap between two users, similar to the results shown in Figure 2. However, examining the entire range of ρ in the cases $N = 1$ and $N = 2$, saturation is attained much more quickly than with $N = 3$, the reason being that a greater number of antennas significantly improves the outage performance.

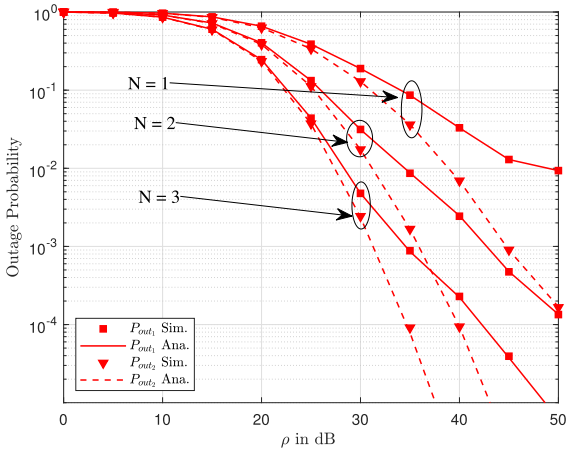

FIGURE 3. Outage probability versus ρ for different values of N, where $\rho_{CU} = 15$dB, $\lambda_g = 0.01$, and the satellite link is set to HS.

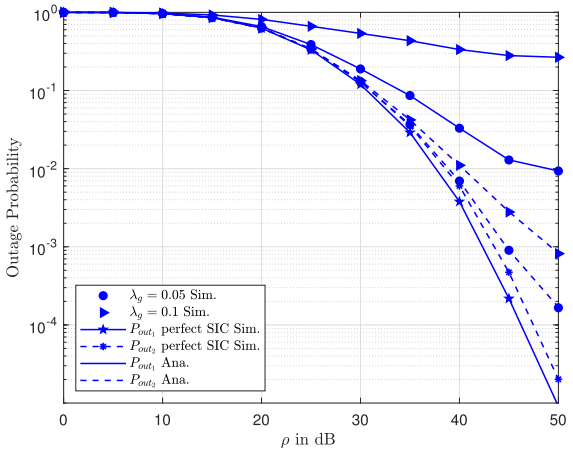

FIGURE 4. Outage probability versus ρ for different values of λ_g, where $N = 1$, $\rho_{CU} = 15$dB, and the satellite link is set to HS.

Figure 4 reveals similar results to the simulations in Figures 2 and 3 and indicates the trends of outage behavior for two users under perfect SIC and ipSIC schemes. When we raise ρ from 40 to 60 dB, the outage performance for perfect SIC is superior to ipSIC, the main reason being that interference from ipSIC limits the SINR, and the corresponding system performance of secondary users is thus reduced. Two levels of the ipSIC case confirm that $\lambda_g = 0.01$ is superior to $\lambda_g = 0.1$.

As with the effect caused by ipSIC, the interference channel of the CUE has an effect on the outage performance of two users (Fig. 5). Here, $\rho_{CU} = 1$ dB produces the corresponding outage probability as the best result of the three considered cases.

Figure 6 shows that when the UAV flies at a greater height, it leads to worse quality in the ground links and consequently worse outage probability for the two users. This can be explained by the distances between the UAV and ground users computed from (1), which depends on the height h. This demonstrates the advantage of the UAV in determining expected system performance. We can achieve the desired performance simply by controlling the height of the UAV.

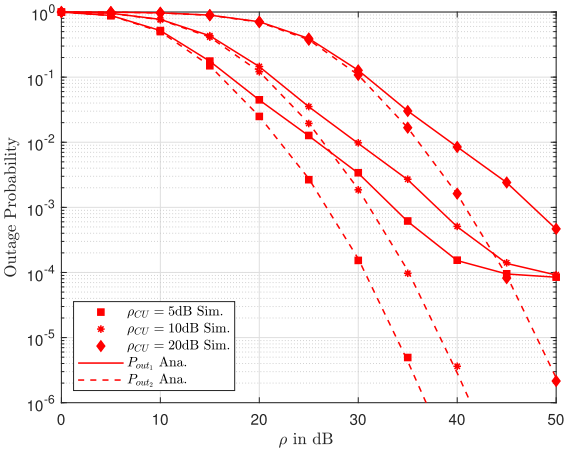

FIGURE 5. Outage probability versus ρ for different values of ρ_{CU}, where $N = 2$, $\lambda_g = 0.01$, and the satellite link is set to HS.

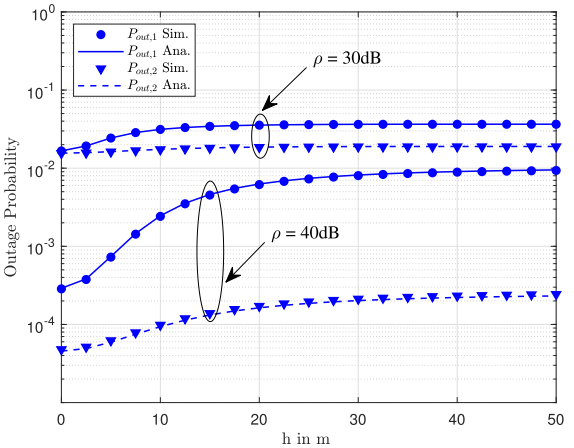

FIGURE 6. Outage probability versus h for different values of ρ, where $N = 2$, $\rho_{CU} = 15$dB, $\lambda_g = 0.01$, and the satellite link is set to HS.

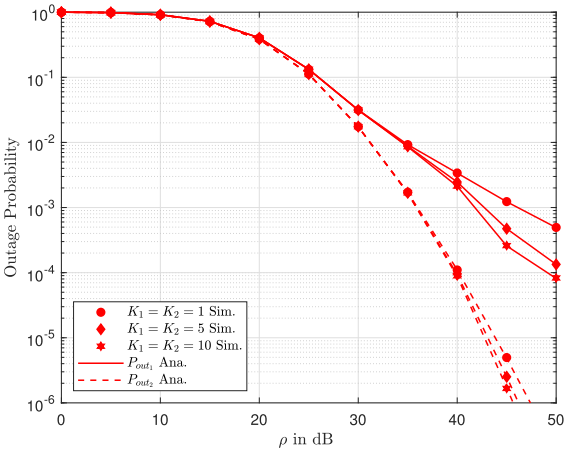

FIGURE 7. Outage probability versus ρ for different values of $K_1 = K_2$, where $N = 2$, $\rho_{CU} = 15$dB, $\lambda_g = 0.01$, and the satellite link is set to HS.

Figure 7 shows that the outage performance can be enhanced significantly under Rician channel conditions. The configuration $K_1 = K_2 = 10$ indicates the best case

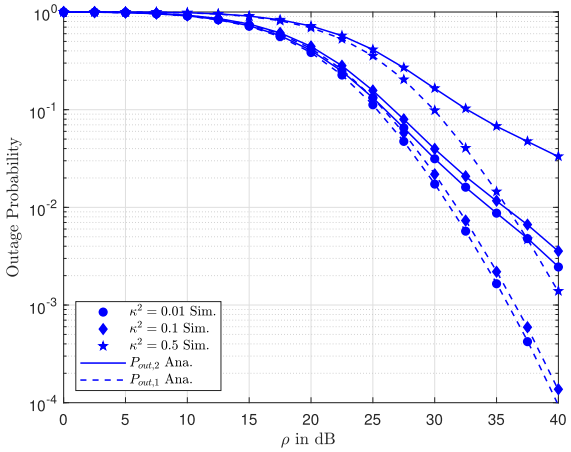

FIGURE 8. Outage probability versus ρ for different values of κ^2, where $N = 2$, $\rho_{CU} = 15$dB, $\lambda_g = 0.01$, and the satellite link is set to HS.

associated with the considered values of the links from the UAV to the ground users, the reason being that the outage probability in (41), (43) contains values of $K_1 = K_2$. The quality of the ground channels plays an important role in altering the outage probability values.

Figure 8 shows the effect of hardware impairment level κ^2 with respect to the outage probability for two users. It is easy to conclude that the lower level of hardware impairment exhibits the best outage performance for two users in the considered system. We note that $\kappa^2 = 0.5$ is a serious degradation in terms of outage for two users. Therefore, a high requirement in perfect hardware design is crucial for maintaining system performance at a desired acceptable quality.

V. CONCLUSION

We investigated the outage probability performance of a UAV-based satellite-terrestrial system with a multi-antenna satellite and NOMA scheme containing hardware impairments and imperfect SIC. To demonstrate the main system performance metric, we derived novel and closed-form expressions of the outage probability. The results showed that the detrimental effects of interference from a non-NOMA user and the deterioration of the outage probability due to imperfect SIC could be mitigated by increasing the number of antennas at the satellite and thus improve system performance. The numerical simulations demonstrated the effect of various key system/channel parameters on the outage probability and provided a guide for the joint deployment of a UAV and multi-antenna satellite in such systems. In future work, it would be interesting to consider multiple antennas at the UAV or even the ground users, providing a more general scenario for study.

APPENDIX A

Using (9) and (10), we write the term Ψ_1, which is shown at the top of the next page, where $\upsilon_1 = \frac{\varphi_1}{Q_1+\varphi_1\kappa^2_{SU_1}}$, $\upsilon_2 = \frac{\varphi_2}{Q_2-\varphi_2\left(Q_1+\kappa^2_{SU_i}\right)}$ and $\upsilon_{\max} = \max(\upsilon_1, \upsilon_2)$.

Based on (19), the term I_1 in (54), as shown at the bottom of the page, can be expressed as

$$I_1 = \sum_{b_1=0}^{m_{SU_1}-1} \cdots \sum_{b_N=0}^{m_{SU_1}-1} \frac{\Xi(SU_1)}{\left(\rho_{SU_1}\right)^{\Lambda}\lambda_{CU_1}} \times \int_0^{\infty} e^{-\frac{x}{\lambda_{CU_1}}} \int_{\upsilon_{\max}(\rho_{CU}x+1)}^{\infty} y^{\Lambda-1} e^{-\frac{\Delta_{SU_1}}{\rho_{SU_1}}y} dy dx. \quad (55)$$

Using [47, eq. 3.351.2], we can express I_1 as

$$I_1 = \sum_{b_1=0}^{m_{SU_1}-1} \cdots \sum_{b_N=0}^{m_{SU_1}-1} \frac{\Xi(SU_1)\, e^{-\frac{\Delta_{SU_1}\upsilon_{\max}}{\rho_{SU_1}}}}{\lambda_{CU_1}\left(\Delta_{SU_1}\right)^{\Lambda-a}} \times \sum_{a=0}^{\Lambda-1} \frac{(\Lambda-1)!}{a!}\left(\frac{\upsilon_{\max}\rho_{CU}}{\rho_{SU_1}}\right)^a \times \int_0^{\infty}\left(x+\frac{1}{\rho_{CU}}\right)^a e^{-\left(\frac{1}{\lambda_{CU_1}}+\frac{\Delta_{SU_1}\upsilon_{\max}\rho_{CU}}{\rho_{SU_1}}\right)x} dx. \quad (56)$$

Then, using [47, eq. 3.382. 4] we rewrite I_1, as expected. The term I_2 is thus expressed as

$$I_2 = \sum_{b_1=0}^{m_{SU_1}-1} \cdots \sum_{b_N=0}^{m_{SU_1}-1} \frac{\Xi(SU_1)\, e^{\frac{1}{\rho_{SU_1}\lambda_g}}}{\left(\rho_{SU_1}\right)^{\Lambda}\lambda_{CU_1}} \int_0^{\infty} e^{-\frac{x}{\lambda_{CU_1}}+\frac{\rho_{CU}}{\rho_{SU_1}\lambda_g}x} \times \int_{\upsilon_{\max}(\rho_{CU}x+1)}^{\infty} y^{\Lambda-1} e^{-\frac{\Delta_{SU_1}}{\rho_{SU_1}}y} e^{-\frac{y}{\upsilon_1\rho_{SU_1}\lambda_g}} dy dx$$

$$\begin{aligned}
\Psi_1 &= 1-\Pr\left(\frac{\beta_{SU_1}Q_2}{\beta_{SU_1}Q_1+\beta_{SU_1}\kappa^2_{SU_1}+\rho_{CU}\left|h_{CU_1}\right|^2+1} > \varphi_2, \frac{\beta_{SU_1}Q_2}{\beta_{SU_1}Q_1+\beta_{SU_1}\kappa^2_{SU_1}+\rho_{CU}\left|h_{CU_1}\right|^2+1} > \varphi_1\right) \\
&= 1-\Pr\left(\beta_{SU_1} > \theta_{\max}\left(\rho_{CU}\left|h_{CU_1}\right|^2+1\right), |g|^2 < \frac{\beta_{SU_1}}{\theta_1\rho_{SU_1}}-\frac{\rho_{CU}\left|h_{CU_1}\right|^2+1}{\rho_{SU_1}}\right) \\
&= 1-\underbrace{\int_0^{\infty} f_{|h_{CU_1}|^2}(x) \int_{\theta_{\max}(\rho_{CU}x+1)}^{\infty} f_{\beta_{SU_1}}(y) dy dx}_{I_1} + \underbrace{\int_0^{\infty} f_{|h_{CU_1}|^2}(x) \int_{\upsilon_{\max}(\rho_{CU}x+1)}^{\infty} f_{\beta_{SU_1}}(y) \int_{\frac{y}{\upsilon_1\rho_{SU_1}}-\frac{\rho_{CU}x+1}{\rho_{SU_1}}}^{\infty} f_{|g|^2}(z) dz dy dx}_{I_2}. \quad (54)
\end{aligned}$$

$$= \sum_{b_1=0}^{m_{SU_1}-1} \cdots \sum_{b_N=0}^{m_{SU_1}-1} \Xi\left(SU_1\right) \sum_{a=0}^{\Lambda-1} \frac{(\Lambda-1)!\left(\upsilon_{\max}\right)^a e^{-\Theta_2}}{\lambda_{CU_1} a!\left(\rho_{SU_1}\right)^a} \times \left(\Delta_{SU_1}+\frac{1}{\upsilon_1\lambda_g}\right)^{-\Lambda+a} \int_0^{\infty} \left(\rho_{CU}x+1\right)^a e^{-\Theta_1 x} dx, \quad (57)$$

where $\Theta_1 = \frac{1}{\lambda_{CU_1}} - \frac{\rho_{CU}}{\rho_{SU_1}\lambda_g} + \frac{\Delta_{SU_1}\upsilon_{\max}\rho_{CU}}{\rho_{SU_1}} + \frac{\upsilon_{\max}\rho_{CU}}{\upsilon_1\rho_{SU_1}\lambda_g}$ and $\Theta_2 = \frac{\Delta_{SU_1}\upsilon_{\max}}{\rho_{SU_1}} + \frac{\upsilon_{\max}}{\upsilon_1\rho_{SU_1}\lambda_g} - \frac{1}{\rho_{SU_1}\lambda_g}$.

Based on [47, eq. 3.382.4], we obtain I_2 as (31).

Substituting (55) and (31) into (54), we obtain the final result.

This ends the proof.

APPENDIX B

First, we denote $A_1 = \Pr\left(\gamma_{SR}^{x_2} > \varphi_2, \gamma_{SR}^{x_1} > \varphi_1\right)$ and $A_2 = \Pr\left(\gamma_{SR}^{x_2} > \varphi_2, \gamma_{SR}^{x_1} > \varphi_1\right)$. Substituting (8) and (9) into A_1, we have (58), as shown at the bottom of the page, where $\theta_1 = \frac{\varphi_1}{Q_1-\varphi_1\kappa_R^2}$, $\theta_2 = \frac{\varphi_2}{Q_2-\varphi_2\left(Q_1+\kappa_R^2\right)}$, $\theta_{\max} = \max\left(\theta_1, \theta_2\right)$.

Based on (19) and [47, eq. 3.351.2], we obtain the term $A_{1,1}$ from

$$A_{1,1} = \sum_{b_1=0}^{m_{SR}-1} \cdots \sum_{b_N=0}^{m_{SR}-1} \frac{\Xi\left(SR\right)}{\left(\Delta_{SR}\right)^{\Lambda}} \Gamma\left(\Lambda, \frac{\Delta_{SR}\theta_{\max}}{\rho_{SR}}\right). \quad (59)$$

Applying (19), we can express $A_{1,2}$ as

$$A_{1,2} = \sum_{b_1=0}^{m_{SR}-1} \cdots \sum_{b_N=0}^{m_{SR}-1} \frac{\Xi\left(SR\right)}{\left(\rho_{SR}\right)^{\Lambda}} e^{\frac{1}{\rho_{SR}\lambda_g}} \times \int_{\theta_{\max}}^{\infty} x^{\Lambda-1} e^{-\left(\frac{\Delta_{SR}}{\rho_{SR}}+\frac{1}{\theta_1\rho_{SR}\lambda_g}\right)x} dx. \quad (60)$$

Similarly, we obtain $A_{1,2}$ from

$$A_{1,2} = \sum_{b_1=0}^{m_{SR}-1} \cdots \sum_{b_N=0}^{m_{SR}-1} \Xi\left(SR\right) \left(\frac{\theta_1\lambda_g}{\Delta_{SR}\lambda_g\theta_1+1}\right)^{\Lambda} \times e^{\frac{1}{\rho_{SR}\lambda_g}} \Gamma\left(\Lambda, \frac{\left(\Delta_{SR}\lambda_g\theta_1+1\right)\theta_{\max}}{\theta_1\rho_{SR}\lambda_g}\right). \quad (61)$$

Applying (12) and (13), A_2 can be calculated as (62), shown at the bottom of the page.

Based on (23), $A_{2,1}$ is rewritten as

$$A_{2,1} = \sum_{b=0}^{\infty}\sum_{c=0}^{b} \frac{\left(K_1\right)^b e^{-K_1}}{b!c!\lambda_{CU_1}} \left(\frac{\tilde{\theta}_{\max}\rho_{CU}\varpi_1}{\rho_{RU_1}}\right)^c e^{-\frac{\varpi_1\tilde{\theta}_{\max}}{\rho_{RU_1}}} \times \int_0^{\infty} \left(x+\frac{1}{\rho_{CU}}\right)^c e^{-\frac{\varpi_1\tilde{\theta}_{\max}\rho_{CU}\lambda_{CU_1}+\rho_{RU_1}}{\rho_{RU_1}\lambda_{CU_1}}x} dx. \quad (63)$$

Based on [47, Eq. 3.382.4], we obtain $A_{2,1}$ from

$$A_{2,1} = \sum_{b=0}^{\infty}\sum_{c=0}^{b} \frac{\left(K_1\right)^b e^{-K_1}\rho_{RU_1}\left(\varpi_1\tilde{\theta}_{\max}\rho_{CU}\lambda_{CU_1}\right)^c}{c!b!\lambda_{CU_1}} \times \frac{e^{-\frac{\varpi_1\tilde{\theta}_{\max}}{\rho_{RU_1}}+\frac{\varpi_1\tilde{\theta}_{\max}\rho_{CU}\lambda_{CU_1}+\rho_{RU_1}}{\rho_{RU_1}\rho_{CU}\lambda_{CU_1}}}}{\left(\varpi_1\tilde{\theta}_{\max}\rho_{CU}\lambda_{CU_1}+\rho_{RU_1}\right)^{c+1}} \times \Gamma\left(c+1, \frac{\varpi_1\tilde{\theta}_{\max}\rho_{CU}\lambda_{CU_1}+\rho_{RU_1}}{\rho_{RU_1}\rho_{CU}\lambda_{CU_1}}\right). \quad (64)$$

$$\begin{aligned} A_1 &= \Pr\left(\frac{\beta_{SR}Q_2}{\beta_{SR}Q_1+\beta_{SR}\kappa_R^2+1} > \varphi_2, \frac{\beta_{SR}Q_1}{\rho_{SR}\left|g\right|^2+\beta_{SR}\kappa_R^2+1} > \varphi_1\right) \\ &= \Pr\left(\beta_{SR} > \theta_{\max}, \left|g\right|^2 < \frac{\beta_{SR}-\theta_1}{\theta_1\rho_{SR}}\right) \\ &= \underbrace{\int_{\theta_{\max}}^{\infty} f_{\beta_{SR}}\left(x\right)dx}_{A_{1,1}} - \underbrace{\frac{1}{\lambda_g}\int_{\theta_{\max}}^{\infty} f_{\beta_{SR}}\left(x\right)e^{-\frac{x-\theta_1}{\theta_1\rho_{SR}}}dx}_{A_{1,2}}, \end{aligned} \quad (58)$$

$$\begin{aligned} A_2 &= \Pr\left\{\beta_{RU_1} > \tilde{\theta}_{\max}\left(\rho_{CU}\left|h_{CU_1}\right|^2+1\right), \left|g\right|^2 < \frac{\beta_{RU_1}}{\tilde{\theta}_1\rho_{RU_1}} - \frac{\left(\rho_{CU}\left|h_{CU_1}\right|^2+1\right)}{\rho_{RU_1}}\right\} \\ &= \underbrace{\int_0^{\infty} f_{\left|h_{CU_1}\right|^2}\left(x\right) \int_{\tilde{\theta}_{\max}\left(\rho_{CU}x+1\right)}^{\infty} f_{\beta_{RU_1}}\left(y\right)dydx}_{A_{2,1}} - \underbrace{\int_0^{\infty} f_{\left|h_{CU_1}\right|^2}\left(x\right) \int_{\tilde{\theta}_{\max}\left(\rho_{CU}x+1\right)}^{\infty} f_{\beta_{RU_1}}\left(y\right) \int_{\frac{y}{\tilde{\theta}_1\rho_{RU_1}}-\frac{\left(\rho_{CU}x+1\right)}{\rho_{RU_1}}}^{\infty} f_g\left(z\right)dzdydx}_{A_{2,2}}. \end{aligned} \quad (62)$$

We then obtain $A_{2,2}$ from

$$A_{2,2} = \sum_{b=0}^{\infty} \frac{(K_1)^b e^{-K_1}}{(b!)^2 \lambda_{CU_1}} \left(\frac{\varpi_1}{\rho_{RU_1}}\right)^{b+1} e^{\frac{1}{\lambda_g \rho_{RU_1}}} \times \int_0^{\infty} e^{-\left(\frac{1}{\lambda_{CU_1}} - \frac{\rho_{CU}}{\lambda_g \tilde{\theta}_1 \rho_{RU_1}}\right)x} \times \int_{\tilde{\theta}_{\max}(\rho_{CU}x+1)}^{\infty} y^b e^{-\left(\frac{\varpi_1}{\rho_{RU_1}} + \frac{1}{\lambda_g \tilde{\theta}_1 \rho_{RU_1}}\right)y} dy dx. \quad (65)$$

We apply a computation similar to (64) and express $A_{2,2}$ as

$$A_{2,2} = \sum_{b=0}^{\infty} \sum_{c=0}^{b} \frac{(K_1)^b (\varpi_1)^{b+1} e^{-K_1}}{b! c! \lambda_{CU_1} \xi^{c+1}} \times \left(\frac{\rho_{CU}\tilde{\theta}_{\max}}{\rho_{RU_1}}\right)^c \left(\frac{\lambda_g \tilde{\theta}_1}{\varpi_1 \lambda_g \tilde{\theta}_1 + 1}\right)^{b-c+1} \times e^{\frac{\xi}{\rho_{CU}} + \frac{1}{\lambda_g \rho_{RU_1}} - \frac{(\varpi_1 \lambda_g \tilde{\theta}_1 + 1)\tilde{\theta}_{\max}}{\lambda_g \tilde{\theta}_1 \rho_{RU_1}}} \Gamma\left(c+1, \frac{\xi}{\rho_{CU}}\right). \quad (66)$$

Based on (59), (61), (64) and (66), we obtain Ψ_2.
This ends the proof.

REFERENCES

[1] X. Yan, K. An, T. Liang, G. Zheng, Z. Ding, S. Chatzinotas, and Y. Liu, "The application of power-domain non-orthogonal multiple access in satellite communication networks," *IEEE Access*, vol. 7, pp. 63531–63539, 2019.
[2] K. An, M. Lin, T. Liang, J.-B. Wang, J. Wang, Y. Huang, and A. L. Swindlehurst, "Performance analysis of multi-antenna hybrid satellite-terrestrial relay networks in the presence of interference," *IEEE Trans. Commun.*, vol. 63, no. 11, pp. 4390–4404, Nov. 2015.
[3] P. K. Upadhyay and P. K. Sharma, "Max-max user-relay selection scheme in multiuser and multirelay hybrid satellite-terrestrial relay systems," *IEEE Commun. Lett.*, vol. 20, no. 2, pp. 268–271, Feb. 2016.
[4] V. Bankey and P. K. Upadhyay, "Ergodic capacity of multiuser hybrid satellite-terrestrial fixed-gain AF relay networks with CCI and outdated CSI," *IEEE Trans. Veh. Technol.*, vol. 67, no. 5, pp. 4666–4671, May 2018, doi: 10.1109/TVT.2018.2793420.
[5] D.-T. Do, T. A. Le, T. N. Nguyen, X. Li, and K. M. Rabie, "Joint impacts of imperfect CSI and imperfect SIC in cognitive radio-assisted NOMA-V2X communications," *IEEE Access*, vol. 8, pp. 128629–128645, 2020.
[6] D.-T. Do, M.-S. Van Nguyen, M. Voznak, A. Kwasinski, and J. N. de Souza, "Performance analysis of clustering car-following V2X system with wireless power transfer and massive connections," *IEEE Internet Things J.*, earl access, Apr. 2, 2021, doi: 10.1109/JIOT.2021.3070744.
[7] X. Yan, H. Xiao, C.-X. Wang, K. An, A. T. Chronopoulos, and G. Zheng, "Performance analysis of NOMA-Based land mobile satellite networks," *IEEE Access*, vol. 6, pp. 31327–31339, 2018.
[8] X. Yue, Y. Liu, Y. Yao, T. Li, X. Li, R. Liu, and A. Nallanathan, "Outage behaviors of NOMA-based satellite network over shadowed-rician fading channels," *IEEE Trans. Veh. Technol.*, vol. 69, no. 6, pp. 6818–6821, Jun. 2020.
[9] X. Zhang, D. Guo, K. An, Z. Chen, B. Zhao, Y. Ni, and B. Zhang, "Performance analysis of NOMA-based cooperative spectrum sharing in hybrid satellite-terrestrial networks," *IEEE Access*, vol. 7, pp. 172321–172329, 2019.
[10] R. Wan, L. Zhu, T. Li, and L. Bai, "A NOMA-PSO based cooperative transmission method in satellite communication systems," in *Proc. IEEE WCSP*, Nanjing, China, Oct. 2017, pp. 1–6.
[11] X. Zhu, C. Jiang, L. Kuang, N. Ge, and J. Lu, "Non-orthogonal multiple access based integrated terrestrial-satellite networks," *IEEE J. Sel. Areas Commun.*, vol. 35, no. 10, pp. 2253–2267, Oct. 2017.
[12] X. Yan, H. Xiao, C.-X. Wang, and K. An, "Outage performance of NOMA-based hybrid satellite-terrestrial relay networks," *IEEE Wireless Commun. Lett.*, vol. 7, no. 4, pp. 538–541, Aug. 2018.
[13] X. Yan, H. Xiao, K. An, G. Zheng, and W. Tao, "Hybrid satellite terrestrial relay networks with cooperative non-orthogonal multiple access," *IEEE Commun. Lett.*, vol. 22, no. 5, pp. 978–981, May 2018.
[14] X. Yan, H. Xiao, K. An, G. Zheng, and S. Chatzinotas, "Ergodic capacity of NOMA-based uplink satellite networks with randomly deployed users," *IEEE Syst. J.*, vol. 14, no. 3, pp. 3343–3350, Sep. 2020.
[15] S. K. Sharma, S. Chatzinotas, and B. Ottersten, "Cognitive radio techniques for satellite communication systems," in *Proc. IEEE 78th Veh. Technol. Conf. (VTC Fall)*, Sep. 2013, pp. 1–5.
[16] W. Liang, S. X. Ng, and L. Hanzo, "Cooperative overlay spectrum access in cognitive radio networks," *IEEE Commun. Surveys Tuts.*, vol. 19, no. 3, pp. 1924–1944, 3rd Quart., 2017.
[17] H. A. Suraweera, P. J. Smith, and M. Shafi, "Capacity limits and performance analysis of cognitive radio with imperfect channel knowledge," *IEEE Trans. Veh. Technol.*, vol. 59, no. 4, pp. 1811–1822, May 2010.
[18] S. K. Sharma, S. Chatzinotas, and B. Ottersten, "Satellite cognitive communications: Interference modeling and techniques selection," in *Proc. 6th Adv. Satell. Multimedia Syst. Conf. (ASMS) 12th Signal Process. Space Commun. Workshop (SPSC)*, Sep. 2012, pp. 111–118.
[19] K. An, M. Lin, W.-P. Zhu, Y. Huang, and G. Zheng, "Outage performance of cognitive hybrid satellite-terrestrial networks with interference constraint," *IEEE Trans. Veh. Technol.*, vol. 65, no. 11, pp. 9397–9404, Nov. 2016.
[20] L. Lv, J. Chen, Q. Ni, Z. Ding, and H. Jiang, "Cognitive non-orthogonal multiple access with cooperative relaying: A new wireless frontier for 5G spectrum sharing," *IEEE Commun. Mag.*, vol. 56, no. 4, pp. 188–195, Apr. 2018.
[21] N.-L. Nguyen, H.-N. Nguyen, A.-T. Le, D.-T. Do, and M. Voznak, "On performance analysis of NOMA-aided hybrid satellite terrestrial relay with application in small-cell network," *IEEE Access*, vol. 8, pp. 188526–188537, 2020.
[22] T. Schenk, *RF Imperfections in High-Rate Wireless Systems: Impact and Digital Compensation*. Berlin, Germany: Springer-Verlag, 2008.
[23] X. Zhang, M. Matthaiou, M. Coldrey, and E. Björnson, "Impact of residual transmit RF impairments on training-based MIMO systems," *IEEE Trans. Commun.*, vol. 63, no. 8, pp. 2899–2911, Aug. 2015.
[24] C. Deng, M. Liu, X. Li, and Y. Liu, "Hardware impairments aware full-duplex NOMA networks over rician fading channels," *IEEE Syst. J.*, vol. 15, no. 2, pp. 2515–2518, Jun. 2021, doi: 10.1109/JSYST.2020.2984641.
[25] K. Guo, K. An, B. Zhang, Y. Huang, and G. Zheng, "Outage analysis of cognitive hybrid satellite-terrestrial networks with hardware impairments and multi-primary users," *IEEE Wireless Commun. Lett.*, vol. 7, no. 5, pp. 816–819, Oct. 2018.
[26] X. Li, J. Li, Y. Liu, Z. Ding, and A. Nallanathan, "Residual transceiver hardware impairments on cooperative NOMA networks," *IEEE Trans. Wireless Commun.*, vol. 19, no. 1, pp. 680–695, Jan. 2020.
[27] X. Tang, K. An, K. Guo, S. Wang, X. Wang, J. Li, and F. Zhou, "On the performance of two-way multiple relay non-orthogonal multiple access-based networks with hardware impairments," *IEEE Access*, vol. 7, pp. 128896–128909, Sep. 2019.
[28] H. Wu, Y. Zou, W. Cao, Z. Chen, T. A. Tsiftsis, M. R. Bhatnagar, and R. C. De Lamare, "Impact of hardware impairments on outage performance of hybrid satellite-terrestrial relay systems," *IEEE Access*, vol. 7, pp. 35103–35112, 2019.
[29] C. Liu, W. Feng, Y. Chen, C.-X. Wang, and N. Ge, "Cell-free satellite-UAV networks for 6G wide-area Internet of Things," *IEEE J. Sel. Areas Commun.*, vol. 39, no. 4, pp. 1116–1131, Apr. 2021.
[30] X. Li, W. Feng, J. Wang, Y. Chen, N. Ge, and C.-X. Wang, "Enabling 5G on the ocean: A hybrid Satellite-UAV-Terrestrial network solution," *IEEE Wireless Commun.*, vol. 27, no. 6, pp. 116–121, Dec. 2020.
[31] P. K. Sharma, D. Gupta, and D. I. Kim, "Cooperative AF-based 3D mobile UAV relaying for hybrid satellite-terrestrial networks," in *Proc. IEEE 91st Veh. Technol. Conf. (VTC-Spring)*, May 2020, pp. 1–5.
[32] P. K. Sharma and D. I. Kim, "Secure 3D mobile UAV relaying for hybrid satellite-terrestrial networks," *IEEE Trans. Wireless Commun.*, vol. 19, no. 4, pp. 2770–2784, Apr. 2020.
[33] J. Ji, K. Zhu, D. Niyato, and R. Wang, "Joint trajectory design and resource allocation for secure transmission in cache-enabled UAV-relaying networks with D2D communications," *IEEE Internet Things J.*, vol. 8, no. 3, pp. 1557–1571, Feb. 2021.

[34] M. Hua, Y. Wang, M. Lin, C. Li, Y. Huang, and L. Yang, "Joint CoMP transmission for UAV-aided cognitive satellite terrestrial networks," *IEEE Access*, vol. 7, pp. 14959–14968, 2019.
[35] J. Yu, X. Liu, Y. Gao, and X. Shen, "3D channel tracking for UAV-satellite communications in space-air-ground integrated networks," *IEEE J. Sel. Areas Commun.*, vol. 38, no. 12, pp. 2810–2823, Dec. 2020.
[36] X. Li, W. Feng, Y. Chen, C.-X. Wang, and N. Ge, "Maritime coverage enhancement using UAVs coordinated with hybrid satellite-terrestrial networks," *IEEE Trans. Commun.*, vol. 68, no. 4, pp. 2355–2369, Apr. 2020.
[37] P. K. Sharma and D. Gupta, "Outage performance of multi-UAV relaying-based imperfect hardware hybrid satellite-terrestrial networks," *IEEE Syst. J.*, early access, Jul. 9, 2021, doi: 10.1109/JSYST.2021.3090799.
[38] X. Tang, K. An, K. Guo, Y. Huang, and S. Wang, "Outage analysis of non-orthogonal multiple access-based integrated satellite-terrestrial relay networks with hardware impairments," *IEEE Access*, vol. 7, pp. 141258–141267, 2019.
[39] P. K. Sharma, D. Deepthi, and D. I. Kim, "Outage probability of 3-D mobile UAV relaying for hybrid satellite-terrestrial networks," *IEEE Commun. Lett.*, vol. 24, no. 2, pp. 418–422, Feb. 2020.
[40] X. Li, Q Wang, H. Peng, H. Zhang, D.-T. Do, K. M. Rabie, R. Kharel, and C. C. Cavalcante, "A unified framework for HS-UAV NOMA networks: Performance analysis and location optimization," *IEEE Access*, vol. 8, pp. 13329–13340, 2020.
[41] S. Lee, D. B. da Costa, Q.-T. Vien, T. Q. Duong, and R. T. de Sousa, "Non-orthogonal multiple access schemes with partial relay selection," *IET Commun.*, vol. 11, no. 6, pp. 846–854, 2017.
[42] V. Bankey, P. K. Upadhyay, D. B. da Costa, P. S. Bithas, A. G. Kanatas, and U. S. Dias, "Performance analysis of multi-antenna multiuser hybrid satellite-terrestrial relay systems for mobile services delivery," *IEEE Access*, vol. 6, pp. 24729–24745, 2018.
[43] Z. Ding, Z. Yang, P. Fan, and H. V. Poor, "On the performance of non-orthogonal multiple access in 5G systems with randomly deployed users," *IEEE Signal Process. Lett.*, vol. 21, no. 12, pp. 1501–1505, Dec. 2014.
[44] M. R. Bhatnagar and M. K. Arti, "Performance analysis of AF based hybrid satellite-terrestrial cooperative network over generalized fading channels," *IEEE Commun. Lett.*, vol. 17, no. 10, pp. 1912–1915, Oct. 2013.
[45] N. I. Miridakis, D. D. Vergados, and A. Michalas, "Dual-hop communication over a satellite relay and shadowed Rician channels," *IEEE Trans. Veh. Technol.*, vol. 64, no. 9, pp. 4031–4040, Sep. 2015.
[46] M. K. Simon and M.-S. Alouini, *Digital Communications over Fading Channels: A Unified Approach to Performance Analysis*. Hoboken, NJ, USA: Wiley, 2000.
[47] I. S. Gradshteyn and I. M. Ryzhik, *Tables of Integrals, Series and Products*, 6th ed. New York, NY, USA: Academic Press, 2000.

NGOC-LONG NGUYEN was born in Binh Dinh Province, Vietnam, in 1973. He received the B.S. and M.S. degrees in physics of electricity from the University of Science, Vietnam. He is currently pursuing the Ph.D. degree with the VSB Technical University of Ostrava, Czech Republic. He is currently working as a Lecturer with the Faculty of Applied Sciences, Ton Duc Thang University. His research interests include applied electronics, satellite systems, non-orthogonal multiple access, and energy harvesting.

SI-PHU LE was born in Da Nang, Vietnam, in October 1985. He received the B.S. degree in information technology from Nha Trang University, and the M.B.A. degree from the Open University of Malaysia. He is currently pursuing the Ph.D. degree with the VSB Technical University of Ostrava, Czech Republic. He was a Lecturer with the Information Technology Department, Van Lang University, for 11 years. He is currently working as the Managing Director at ACEXIS JSC. His research interests include applied wireless communication, cognitive radio, and energy harvesting.

ANH-TU LE (Student Member, IEEE) was born in Lam Dong, Vietnam, in 1997. He is currently pursuing the Ph.D. degree in communications and information systems in wireless systems. He is currently a Research Assistant at WICOM Lab in Industrial University of Ho Chi Minh City, Vietnam. He has authored or coauthored over five articles published in peer-reviewed international journals. His research interests include wireless channel modeling, NOMA, cognitive radio, and MIMO.

NHAN DUC NGUYEN received the M.Eng. degree in electronic materials from the International Training Institute for Materials Science (ITIMS), Hanoi University of Technology, in 1998, and the Ph.D. degree in electrical and computer systems engineering from Monash University, Australia, in 2011. Since 1999, he has been with the Faculty of Telecommunications, Post and Telecommunication Institute of Technology, Vietnam, as a Lecturer. He served as the Head of the Signals and Systems Department, Post and Telecommunication Institute of Technology, from 2014 to 2020. He is currently serving as a Systems Engineering Director of the Innovation Center, Van Lang University. His research interests include optical communications, numerical modeling and analysis, signal processing, and sensor data processing in machine learning.

DINH-THUAN DO (Senior Member, IEEE) received the B.S., M.Eng., and Ph.D. degrees from Vietnam National University (VNU-HCMC), in 2003, 2007, and 2013, respectively. His studies specialized in communications engineering. Prior to joining Asia University, he was an Assistant Professor with Ton Duc Thang University and a Senior Engineer at the VinaPhone Mobile Network, from 2003 to 2009. He has published one sole author book, one edited book, and six book chapters. He has authored or coauthored over 100 technical papers published in peer-reviewed international journals (SCIE) and over 60 conference papers. His research interests include signal processing in wireless communications networks, MIMO, NOMA, UAV networks, satellite systems, physical layer security, device-to-device transmission, and energy harvesting. He is a recipient of the Golden Globe Award from the Vietnam Ministry of Science and Technology, awarded in 2015 (top ten most excellent scientists nationwide). He also received the Creative Young Medal, in 2015. He has presented as a lead guest editor in several special issues in peer-reviewed journals. He serves as an Associate Editor in five SCIE journals.

MIROSLAV VOZNAK (Senior Member, IEEE) received the Ph.D. degree in telecommunications from the Faculty of Electrical Engineering and Computer Science, VSB Technical University of Ostrava, in 2002, and the habilitation degree, in 2009. He was appointed as a Full Professor in electronics and communications technologies, in 2017. He is currently the Principal Investigator with the Research Project QUANTUM5 funded by NATO, which focuses on the application of quantum cryptography in 5G campus networks. He has authored or coauthored over one hundred articles in SCI/SCIE journals. His research interests include ICT, especially on the quality of service and experience, network security, wireless networks, and big data analytics. According to the Stanford University study released, in 2020, he is one of the world's top 2% of scientists in networking and telecommunications and information and communications technologies. He served as the General Chair of the 11th IFIP Wireless and Mobile Networking Conference, in 2018, and the 24th IEEE/ACM International Symposium on Distributed Simulation and Real Time Applications, in 2020. He participated in six projects funded by the EU in programs managed directly by the European Commission.